Enhanced electrochemical performance of RuO_2 doped $LiNi_{1/3}Mn_{1/3}Co_{1/3}O_2$ cathode material for Lithium-ion battery

K. Kalaiselvi
Alagappa University
S. Premlatha
JSU: Jiangsu University
M. Raju
Central Electrochemical Research Institute CSIR
Paruthimal Kalaignan Guruvaiah (pkalaignan@yahoo.com)
Alagappa University https://orcid.org/0000-0002-8372-6389

Research Article

Keywords: LiNi1/3Mn1/3Co1/3O2, RuO2, Cathode materials, sol-gel method, doping

Posted Date: February 24th, 2021

DOI: https://doi.org/10.21203/rs.3.rs-225914/v1

Abstract

$LiNi_{1/3}Mn_{1/3}Co_{1/3}O_2$ as a promising cathode material for lithium-ion batteries was synthesized by a sol-gel method using nitrate precursor calcined at 800°C for 10 hours. The crystallite nature of samples is confirmed from X-ray diffraction analysis. SEM and TEM analyses were used to investigate the surface morphology of the prepared samples. It was found that, highly crystalline polyhedral RuO_2 nanoparticles are well doped on the surface of pristine $LiNi_{1/3}Mn_{1/3}Co_{1/3}O_2$ with a size of about approximately 200 nm. The chemical composition of the prepared samples was characterized by EDX and XPS analyses. The electrochemical performance of the proposed material was studied by cyclic voltammetry and charge/discharge analyses. The electrode kinetics of the samples was studied by electrochemical impedance spectroscopy. The developed RuO_2 doping may provide an effective strategy to design and synthesize the advanced electrode materials for lithium ion batteries. The doping strategy has dramatically increased the capacity retention from 74 % to 90% with a high discharge capacity of 251.2 $mAhg^{-1}$. 3 % RuO_2-doped $LiNi_{1/3}Mn_{1/3}Co_{1/3}O_2$ cathode materials have showed the similar characteristics of two potential plateaus obtained at 2.8 and 4.2 V compared with un doped electrode cathode material. These results revealed the enhanced performance of RuO_2- doped $LiNi_{1/3}Mn_{1/3}Co_{1/3}O_2$ during insertion and extraction of lithium ions compared to pristine material.

Introduction

Increasing demand for portable electronics and electric vehicles has attracted immense interest in Li-ion batteries research as it is considered as a promising electric storage technology for upcoming electric vehicles (EV) and renewable energy power stations owing to its high capacity and low cost [1–5]. Previously, $LiCoO_2$ has ruled over the lithium ion market due to its ease of fabrication and cycling performance. However, the safety concerns of cobalt and requirements of high potentials stimulated the research towards the alternative positive materials [6]. At present, olivine $LiFePO_4$, spinel $LiMn_2O_4$, Li-Mn-rich layered oxides has been widely used in lithium ion batteries. But, the low voltage and low capacity of the above materials and high cost impedes its wide usage. [7, 8]. Hence the layered $LiNi_{0.3}Mn_{0.3}Co_{0.3}O_2$ cathode materials gained more focus and are more attractive due to the high theoretical specific capacity, relatively low cost and better thermal stability [9, 10]. The successful application of these materials can increase the energy density of Li-ion batteries, such as $LiNi_{0.3}Mn_{0.3}Co_{0.3}O_2$ (LNMC), delivered a higher capacity more than 250 $mAhg^{-1}$ when they are charged at higher potentials greater than 4.2 V [11]. $LiNi_{0.3}Mn_{0.3}Co_{0.3}O_2$ (LNMC) has attracted immense research interest in the fabrication of Li-ion batteries. Many researchers have reported the improved performance of this cathode material by adopting various strategies [12–16]. Some of them are surface coating, ion doping, wet chemical synthesis, particle size reducing and so on. Among them, metal ion doping is a facile method to improve the electrochemical properties of cathode material. The electrochemical performance needs to be improved, especially for the development of electric vehicles. On the other hand, the radius of the lithium ion (0.76 nm) is close to the radius of the nickel ion (0.69 nm). Therefore, the cation disorder tends to happen between the nickel ions

and lithium ions [17]. The higher cation disorder would make it more difficult for lithium ions to de-intercalate from the layered structure, resulting in a loss of electrochemical performance. So the content of Ni can affect the electrochemical performance of the layered lithium–nickel– manganese–cobalt oxide materials dramatically. Therefore, the modification on nickel may improve structural ordering and electrochemical performance.

The doped compounds or elements into the cathode materials, such as Sm, Y, Al_2O_3, Nb, W etc [18–23] has been studied by many people. Doping can change both structure and/or morphology, as the doped elements enter into the crystal lattice of the cathode materials. The lattice parameters may also be changed after the crystal lattice has had more kinds of elements. S. C. Yin et al studied the X-ray/Neutron diffraction and lithium De/Re intercalation in $Li_{1-x}Co_{1/3}Ni_{1/3}Mn_{1/3}O_2$ [24]. The electrochemical properties may improve after modification, and the electrochemical properties will also then be improved. Recently, the applications of RuO_2 in LIBs have engendered substantial interest owing to their high surface area and electronic conductivity. Cathode materials doped by RuO_2 haven't studied in detail. Here, we expect RuO_2 would improve the structure-property relationship, lower the cation disorder and enhance the electrochemical performance of the cathode material $LiNi_{0.3}Mn_{0.3}Co_{0.3}O_2$. In this work, a series of RuO_2 doped $LiNi_{0.3-}Mn_{0.3}Co_{0.3}O_2$ (RuO_2-LNMC) materials were prepared, and the effects of doping on the structure, morphology, and electrochemical performance of the LNMC cathode materials were compared. The SEM, TEM, and XRD techniques were employed to investigate the effect and mechanism of doped cathode material.

Experimental Details

Chemicals

All experiments in this work were carried out using analytical grade chemicals without further purification. Metal precursors such as Lithium nitrate ($LiNO_3$), Nickel (II) nitrate ($Ni(NO_3)_2$, Cobalt (II) nitrate hexahydrate $Co(NO_3)_{2.}6H_2O$, manganese (II) nitrate ($Mn(NO_3)_2$ and Ruthenium (III) chloride hydrate ($RuCl_3$) chemicals and aluminum foil (0.025mm thickness) were purchased from Alfa Aesar. All aqueous solutions in this work were prepared with millipore water.

Synthesis of Ru-LNMC (Ruthenium doped ($LiNi_{1/3}Mn_{1/3}Co_{1/3-x})O_2$)

The $LiNi_{1/3}Mn_{1/3}Co_{1/3}O_2$ cathode material was synthesized by the citric acid-assisted sol-gel method and the preparation procedure is schematically illustrated in Fig.1. The stoichiometric amount of $LiNO_3$, and equimolar concentration (0.3 M) of ($Ni(NO_3)_2$, $Co(NO_3)_{2.}6H_2O$, and $Mn(NO_3)_2$ were dissolved in 100 ml deionized water and then 1M of citric acid solution (50 ml) was added drop wise into the above solution and stirred well by using the magnetic stirrer at 80^oC. Citric acid was used as a chelating agent in the reaction system. Ammonium hydroxide (NH_4OH) was added to adjust the pH to 9. Then the reaction continued to form a viscous gel. The resulting gel was dried in hot air oven at 120^oC for 8 h to obtain

pristine $LiNi_{1/3}Mn_{1/3}Co_{1/3}O_2$ in powder form. The obtained powder was calcined at 800^oC for 10 h under air atmosphere in a muffle furnace and then allowed to cool naturally to room temperature. The final product was ground into fine powder using a mortar and kept in a desiccator for further use.

For doping RuO_2 with the pristine material, previously synthesized pristine $LiNi_{1/3}Mn_{1/3}Co_{1/3}O_2$ was mixed with $RuCl_3$ in different ratios such as 1, 2 and 3% were dispersed in ethanol and kept for stirring. 100 ml of ammonium hydroxide (NH_4OH) was added drop wise to start the precipitation process of ruthenium hydroxide on to the surface of pristine material. After the completion of precipitation, the obtained product was washed with copious amount of water to remove the unreacted chloride ions. Resultant powder was dried at 180°C and further subjected to heat treatment at 600°C for 12 hours to get the RuO_2 doped $LiNi_{1/3}Mn_{1/3}Co_{1/3}O_2$.

Electrode preparation and Coin cell assembly

To examine the electrochemical properties of RuO_2 doped $LiNi_{1/3}Mn_{1/3}Co_{1/3}O_2$, standard 2032 Coin type cells were assembled under argon atmosphere in a glove box. In a typical procedure, doctor blade method was used to prepare the proposed cathode material. The slurry was prepared with a proportion of 80 weight % of active materials 10 weight % of conductive acetylene black and 10 weight % of PVDF binder dissolved in N-methyl 2-Pyrrolidone (NMP) solvent. The paste was then applied on the aluminum foil current collector and then dried at 120^oC for 12 h in a hot air oven. The working electrodes were prepared by loading the cutting disc films with a diameter of 1.0 cm into the cleaned and polished aluminum meshes, and then they were pressed under the pressure of 10 MPa for 1 minute to fabricate the cathode material. Lithium sheet (China Energy Lithium Co., Ltd) was served as the negative electrode, and commercial polyethylene (PE) micro porous film (ND420H129-100, Asahi Kasei Chemical Co.) was used as a separator. The electrolyte solution was 1 mol dm^{-3} $LiPF_6$ dissolved in a mixture of ethylene carbonate and dimethyl carbonate (1:1 by volume).The galvanostatic charge/discharge cycles were carried out at a current density of 20 mA g^{-1} in the voltage range from 2.5 to 4.2 V on a battery testing system (CT2001A, Wuhan LAND Electronics Co., Ltd) at room temperature. The electrochemical studies were carried out at room temperature on an Autolab PGSTAT30 Potentiostat/Galvanostat electrochemical workstation (EcoChemi, Netherlands) at a scan rate of 0.1 mV s^{-1} in the potential range between 2.5 and 4.2 V.

Characterization

The surface morphology and the crystallite size were observed from scanning electron microscopy (SEM) using FEI Quanta 250 (FEI Corporation, Japan) instrument, and transmission electron microscopy (TEM) (200kV FEI Tecnai F20). The crystal planes and their structure of the proposed battery material were studied from X-ray diffraction patterns using Rigaku Ultima IV (USA) fully automatic high resolution X-ray diffractometer by employing Cu-K_α (λ=1.54Å) radiation. The elemental composition was studied by using XPS (ESCALAB 250xi, Thermo Scientific) and EDX analysis associated with SEM. The charge transfer

resistance R_{ct} values were derived from Electrochemical Impedance spectroscopy. The discharge capacity of $LiNi_{1/3}Mn_{1/3}Co_{1/3}O_2$ and RuO_2 doped samples was studied using charge discharge curves.

Results And Discussion

X-ray diffraction analysis

Fig 2 displays the XRD patterns for pristine $LiNi_{1/3}Mn_{1/3}Co_{1/3}O_2$ and RuO_2 doped $LiNi_{1/3}Mn_{1/3}Co_{1/3}O_2$. As seen in Fig 1a, the peak positioned at 2θ = 18.7, 44.5, 49.5, 36.6 and 66.2 are consistent with (003), (104), (105), (101) and (108) crystal planes of $LiNi_{1/3}Mn_{1/3}Co_{1/3}O_2$ and the preferred orientation is being at (104) plane. But for the other three RuO_2 doped material which exhibited the similar XRD pattern with enhanced peak intensities suggested the existence of better crystal structure. A weak peak diffracted at 2 theta value of 28.2 is due to the presence of RuO_2 on the surface of $LiNi_{1/3}Mn_{1/3}Co_{1/3}O_2$ is shown in Fig 1(b-d). However, the weak intense peaks at 43.20 and 63.40 indicate the cubic structured phase of $LiNiO_2$. For all the samples, the diffraction peaks were sharp and well definite revealed the good crystallinity and the crystal structure was recognized as a hexagonal α-$NaFeO_2$ structure with R3m space group [25,26] that approves the occurrence of layers of Li, Ni, Mn, and Co in a single-phase layered structure. 3wt % RuO_2 doped sample exhibited higher intensity crystal planes than that of other samples indicating the importance of RuO_2 and good crystallinity.

Surface morphology analysis

SEM characterization was used to study the morphology of pristine $LiNi_{1/3}Mn_{1/3}Co_{1/3}O_2$ and RuO_2 doped $LiNi_{1/3}Mn_{1/3}Co_{1/3}O_2$ samples and are shown in Fig 3. All the samples presented in the SEM images are well-crystalline polyhedral nanoparticles with a size of about approximately 200 nm. As seen in Fig 3a, pristine $LiNi_{1/3}Mn_{1/3}Co_{1/3}O_2$ showed a layered structure with high uniformity and is in good agreement with the previous reports [27]. In the case of 3 wt% RuO_2 doped samples, RuO_2 nanoparticles are entrapped on the surface of pristine $LiNi_{1/3}Mn_{1/3}Co_{1/3}O_2$ that may be due to the high surface energy of the nanoparticles forming a surface doped layer which is shown as in Fig 3b. On increasing the concentration of RuO_2 (3 %), the coatings become more compact. It is clear that, all the RuO_2 doped samples showed a rough surface than that of pristine material. This rough surface may enhance the electronic conductivity of the Li-rich material, lowering the ion diffusion resistance, providing a stable protective structure for the bulk material, and avoiding the occurrence of surface side reactions between the electrode material and electrolyte.

In order to get further insight about the surface morphology, TEM analysis was carried out. Fig 4a shows the formation of similar polyhedral morphology as observed in SEM picture. The introduction of 3 % of RuO_2 does not show any significant morphological changes but the embedded nanoparticles are clearly seen in Fig 4b.The crystalline size of the nanoparticles is estimated as approximately 200 nm. The corresponding SAED pattern shows the ring pattern along with bright spots suggested the poly crystalline

nature of the proposed battery material is shown in Fig 4c. Lattice fringes are also well agreed with the crystal planes and are shown as Fig. 4d. The wider fringe spacing is 0.47 nm for the (003) planes of the layered structure, and the slightly finer lattice fringe is 0.30 nm for the (111) planes of the rutile structured RuO_2. However, the fringe spacing of RuO_2 is lower than that of pure RuO_2 crystals (0.31 nm), which is ascribed to the doped Ru element.

EDX analysis

The chemical composition of RuO_2 doped $LiNi_{1/3}Mn_{1/3}Co_{1/3}O_2$ was studied from energy dispersive X-ray spectroscopy (EDX) Fig. 5. The EDX spectrum reveals the existence of Ni, Mn, Co O and Ru elements in the Li-rich material with the wt% of 18.6, 19.4, 25.6, 31.1 and 8.1 respectively. Inset shows the actual weight % of the elements such as Li, Ni, Co, Mn, and O along with Ru indicating that the surface of $LiNi_{0.23}$ $Ru_{0.1}Mn_{0.33}Co_{0.33}O_2$ is decorated with RuO_2 nanoparticles.

XPS analysis

The XPS technique was used to investigate the elemental composition of the as-prepared material and the valence states of elements (Fig 6). However, it can be found that the orbital binding energy of Ni $2p_{3/2}$ is located at 851 eV in Fig. 6a which significantly shifts to higher binding energy positions (856 eV) indicating that a part of Ni^{2+} turns into higher valence state. According to this result, it could be concluded that partial Ru^{4+} ions enter the crystalline lattice of the $LiNi_{1/3}Mn_{1/3}Co_{1/3}O_2$ material and replace a part of Ni^{2+} ions. From the XPS spectra of Ru 3p, it can be seen that the main peaks at about 465.3, 462.8 eV correspond to Ru $3p_{5/2}$ and Ru $3p_{3/2}$ signals of Ru^{4+} and Ru^{3+} respectively [28] with no significant chemical shift. The addition of Ru promotes the generation of more number of oxygen vacancies. In addition, it also facilitates the redox reaction between Ru^{4+} and Ru^{3+} of RuO_2 and further enhances its oxygen storage capacity. The two main peaks centered at 781.1 eV and 797.2 eV are due to the $2p_{3/2}$, $2p_{1/2}$ spin orbit splitting of cobalt respectively [29]. The more oxygen vacancies were also verified using O 1s spectra of the as-prepared materials. In view of the analysis, the peaks located at 529.2 and 531.2 eV were assigned to lattice oxygen, oxygen vacancies, and chemisorbed oxygen, respectively [30]. Obviously, the content of oxygen vacancies is further increased after the incorporation of Ru. It is clear that Ru doped $LiNi_{1/3}Mn_{1/3}Co_{1/3}O_2$ possesses more oxygen vacancies, which is favorable for promoting the activation of $LiNi_{1/3}Mn_{1/3}Co_{1/3}O_2$. From the above results, it can be concluded that Ru^{4+} ions incorporated into the pristine material was expected to enhance the electrochemical performance of the material.

Electrochemical Impedance spectroscopy

Electrochemical Impedance spectroscopy is used to study the kinetics during lithium intercalation/deintercalation process. Fig 7 shows the electrochemical impedance spectroscopy (EIS) profile of pristine $LiNi_{1/3}Mn_{1/3}Co_{1/3}O_2$ and RuO_2 doped $LiNi_{1/3}Mn_{1/3}Co_{1/3}O_2$. The impedance spectrum

consists of a semicircle in the intermediate frequency ranges followed by an inclined straight line at the low frequency range. In general, the semicircle in the high to medium frequency region is related to the charge transfer resistance (R_{ct}) [31,32] and in the low frequency region represents the Warburg impedance (Z_w), which is ascribed to Li-ion diffusion in the solid phase state of the electrode material. According to Fig 7, the R_{ct} value of the RuO_2 doped electrode is smaller than that of the un doped pristine electrode. The diameter of the semicircle for the un doped electrode is 226.79 Ω and that of the doped electrode is 205.47 Ω. Since the diameter decreases for the RuO_2 doped electrode has confirmed the enhancement of conductivity. As a consequence, the electrochemical properties get improved. The equivalent circuit is shown as inset in Fig 7.

Electrochemical performance of RuO_2 doped $LiNi_{1/3}Mn_{1/3}Co_{1/3}O_2$ cathode material

The electrochemical performance of the proposed battery material was investigated by galvanostatic charge/discharge curves at 0.1 C rates in the voltage range between 2.8 to 4.2 V. As seen in Fig 8, the charge/discharge curve plateaus meets at around 3.9 V and the potential drop was observed at 3.6 V warrants the higher energy density. In general, the wider charge/discharge profile suggests the better stability of the electrode. The discharge capacity for the pristine material was estimated as 194.9 $mAhg^{-1}$ whereas for 1, 2 and 3 wt % of RuO_2 doped $LiNi_{1/3}Mn_{1/3}Co_{1/3}O_{2,}$ the discharge capacity values are calculated as 214.9, 242.9, and 251.2 $mAhg^{-1}$ respectively. As expected, 3 wt % RuO_2 doped sample exhibits better cyclic performance compared to other electrodes which is well agreed with the literature [33]. The embedded RuO_2 particles suppress the metal ion dissolution and unwanted side reaction between the electrode and electrolyte leads to the enhanced Li transportation. Consequently, rate performance of the proposed cathode material was improved. After 100 cycles, 3.2 % capacity fade was observed for 3% RuO_2 doped sample which may be due to the dissolution of transition metal ions at higher voltage or the electrolyte decomposition.

In order to test the electrode stability and capacity retention, galvanostatic charge /discharge test was carried out (Fig 9). All the electrodes were charged and discharged at 0.1 C rates between 2.8 to 4.2 V for 100 cycles. For the pristine $LiNi_{1/3}Mn_{1/3}Co_{1/3}O_{2,}$ the initial discharge capacity is 194.9 $mAhg^{-1}$, and after 100 cycles the discharge capacity is reduced to 143.27$mAhg^{-1}$ and 74 % of capacity was retained. In the case of 1% of RuO_2 doped $LiNi_{1/3}Mn_{1/3}Co_{1/3}O_{2,}$ 75 % capacity retention was obtained whereas for 2% RuO_2 doped material capacity remains as 217 $mAhg^{-1}$ and the retention is 89 %. 3% RuO_2 doped $LiNi_{1/3}Mn_{1/3}Co_{1/3}O_2$, shown better capacity retention and long lasting stability. The initial discharge capacity is 251.2 $mAhg^{-1}$ and it was slightly declined to 226 $mAhg^{-1}$ after 100 cycles indicating the superior performance of the proposed cathode material. The doping strategy revealed the better performance than the previous reports [34]. The capacity retention was determined as 90 %. The addition of RuO_2 facilitates the transportation of Li^{2+} ions in the electrode-electrolyte interface. The existence of Ru in crystal lattice could enhance the ability of Li diffusion, more Li ions can be easily extracted from Li layers. Consequently, higher extent of phase transformation from layered Li_2MnO_3 to certain spinel-like

regions could be expected. As a consequence, capacity caused by reinsertion of Li ions into local transformed spinel-like regions during discharge will be increased. Another reason for the higher capacity contribution from spinel-like regions is that the appropriate amount of Ru (x = 0.01) gives rise to a certain impact on transferred spinel-like lattice to enhance Li diffusivity in these regions [35]. It is worth mentioning that, on increasing the cycle numbers the specific capacity also increases owing to the good activation of the electrodes.

Cyclic Voltammetry is a useful method for determining the structural changes in Lithium intercalation/deintercalation process. To get further information about the electrochemical characteristics, Cyclic Voltammetry experiments were performed in the scan range of 2.8 to 4.2 V at a scan rate of 1 mVs^{-1}. Cyclic voltammograms of first six cycles of RuO_2 doped $LiNi_{1/3}Mn_{1/3}Co_{1/3}O_2$ is shown in Fig 10. A double layer capacitive behavior was observed rather than the typical redox behavior of RuO_2.

Conclusions

Herein we report the facile synthesis of $LiNi_{1/3}Mn_{1/3}Co_{1/3}O_2$ and RuO_2 doped $LiNi_{1/3}Mn_{1/3}Co_{1/3}O_2$ with different weight percentage and demonstrated their improved battery performance for Lithium ion batteries. The proposed samples were characterized by different characterization techniques. The structural elucidation was done by XRD analysis. The surface morphology and chemical composition was studied by TEM and XPS analyses respectively. The stability and the capacity retention were investigated by using galvanostatic charge/discharge curves. About 226 $mAhg^{-1}$ discharge capacity was retained after 100 cycles suggested the high specific capacitance and good cyclic stability of the proposed electrode material. This may be attributed to the presence of RuO_2 doped layer which reduce the barrier for lithium transfer between the electrode-electrolyte interfaces. In addition, the abundant oxygen vacancies in the doped layer significantly facilitate the activation the electrode during the initial charging process. Besides, the reduced oxygen loss can effectively inhibit the decomposition of the electrolyte and protect the active substances from being dissolved, thus forming a thin and stable film. Therefore, the newly developed 3% RuO_2 doped on pristine $LiNi_{1/3}Mn_{1/3}Co_{1/3}O_2$ may provide an effective strategy to design and synthesize advanced electrode materials for future energy storage devices

Declarations

Acknowledgement

The first author would like to thank the Department of Science and Technology (DST), New Delhi, for providing financial assistance under the DST-INSPIRE Program. The authors also thank the DST-Nano mission, DST – PURSE–II and MHRD – RUSA – 2.0, New Delhi for providing financial assistance to carry out this research work.

References

1. J. Zhu, L. Lu, K. Zeng, Nanoscale mapping of lithium-ion diffusion in a cathode within an all-solid-state lithium-ion battery by advanced scanning probe microscopy techniques. ACS Nano **2**, 1666–1675 (2013)
2. T. Zhao, S. Chen, L. Li, X. Zhang, H. Wu, T. .Wu, C.J. Sun, R. Chen, F. Wu, J. Lu, Organic-acid-assisted fabrication of low-cost Li-rich cathode material (Li $[Li_{1/6}Fe_{1/6}Ni_{1/6}Mn_{1/2}]$ O_2) for lithium–ion battery. ACS Appl. Mater. Interfaces **6**, 22305–22315 (2014)
3. Y.F. Deng, S. X.Zhao, Y.H. Xu, K. Gao, CW .Nan. Impact of P-doped in spinel $LiNi_{0.5}Mn_{1.5}O_4$ on degree of disorder, grain morphology, and electrochemical performance. Chemistry of Materials. **27**, 7734–7742 (2015)
4. M. Gu, I. Belharouak, J. Zheng, H. Wu, J. Xiao, A. Genc, K. Amine, S. Thevuthasan, D.R. Baer, J.G. Zhang, N.D. Browning, Formation of the spinel phase in the layered composite cathode used in Li-ion batteries. ACS Nano **7**, 760–767 (2013)
5. H. X.Chen, Y.C. Zhu, Y. .Chen, A. Shang, L. .Cao, G.W. Hu, Rubloff, MWCNT/V_2O_5 core/shell sponge for high areal capacity and power density Li-ion cathodes. ACS Nano **6**, 7948–7955 (2012)
6. W. Luo, X. Li, J.R. Dahn, Synthesis, characterization, and thermal stability of Li $[Ni_{1/3}Mn_{1/3}Co_{1/3-z}$ (MnMg) $z/_2]$ O_2. Chem. Mater. **22**, 5065–5073 (2010)
7. L. Li, L. Wang, X. Zhang, M.Xie,F. .Wu, R. Chen, Structural and electrochemical study of hierarchical $LiNi_{1/3}Co_{1/3}Mn_{1/3}O_2$ cathode material for lithium-ion batteries. ACS Appl. Mater. Interfaces **7**, 21939–21947 (2015)
8. L.S. Cahill, S.C. Yin, A. Samoson, I. Heinmaa, L.F. Nazar, GR. Goward. ^{6}Li NMR studies of cation disorder and transition metal ordering in $[LiNi_{1/3}Co_{1/3}Mn_{1/3}]$ O_2 using ultrafast magic angle spinning. Chemistry of materials **17**, 6560–6566 (2005)
9. Z. J.Zhang, R. Li, Z. .Gao, Hu, X .Liu. High rate capability and excellent thermal stability of Li^+-conductive Li_2ZrO_3-coated $LiNi_{1/3}Co_{1/3}Mn_{1/3}O_2$ via a synchronous lithiation strategy. J. Phys. Chem. C **119**, 20350–20356 (2015)
10. E. Zhao, M.Chen,D. .Chen, X. .Xiao, Z. Hu, A versatile coating strategy to highly improve the electrochemical properties of layered oxide LiMO2 (M = $Ni_{0.5}Mn_{0.5}$ and $Ni_{1/3}Mn_{1/}$. ACS Appl. Mater. Interfaces **7**($_3Co_{1/3}$), 27096–27105 (2015)
11. C. Liu, Z.Wang,C. .Shi, E. .Liu, C. .He, N. Zhao, Nano structured hybrid layered-spinel cathode material synthesized by hydrothermal method for lithium-ion batteries. ACS applied materials & interfaces. **6**, 8363–8368 (2014)
12. L. Li, L. Wang, X. Zhang, M. Xie, ,F. .Wu, R. Chen, Structural and electrochemical study of hierarchical $LiNi_{1/3}Co_{1/3}Mn_{1/3}O_2$ cathode material for lithium-ion batteries. ACS Appl. Mater. Interfaces **7**, 21939–21947 (2015)

13. L. Yao, Y. Feng, G. Xi, A new method for the synthesis of $LiNi_{1/3}Co_{1/3}Mn_{1/3}O_2$ from waste lithium ion batteries. RSC Advances **5**, 44107–44114 (2015)
14. Q. Jiang, L. Xu, J. Huo, H.Zhang,S. Wang, Plasma-assisted highly efficient synthesis of Li ($Ni_{1/3}$ $Co_{1/3}$ $Mn_{1/3}$) O_2 cathode materials with superior performance for Li-ion batteries, RSC Advances, Chem. Commun, 1–3(2015)
15. Y. Wu, C. Cao, Y. Zhu, J. Li, L. Wang, Cube-shaped hierarchical $LiNi_{1/3}Co_{1/3}Mn_{1/3}O_2$ with enhanced growth of nanocrystal planes as high-performance cathode materials for lithium-ion batteries. Journal of Materials Chemistry A **0.0**, 1–3 (2012)
16. J.H. Lee, J.W. .Kim, H.Y. Kang, S.C. Kim, S.S. .Han, K.H. .Oh, S.H. .Lee, Y.C. Joo, The effect of energetically coated ZrO_x on enhanced electrochemical performances of Li ($LiNi_{1/3}Co_{1/3}Mn_{1/3}$) O_2 cathodes using coated radio frequency (RF) sputtering. Journal of Materials Chemistry A **3**, 12982–12991 (2015)
17. P.S. Whitfield, I.J. Davidson, L.M.Cranswick,I.P. .Swainson, P.W. Stephen, Investigation of possible superstructure and cation disorder in the lithium battery cathode material $LiNi_{1/3}Co_{1/3}Mn_{1/3}O_2$ using neutron and anomalous dispersion powder diffraction. Solid State Ionics **176**, 463–471 (2005)
18. Y. Kim, H. Kim, S.W. Martin, Synthesis and electrochemical characteristics of Al_2O_3-coated $LiNi_{1/3}Co_{1/3}Mn_{1/3}O_2$ cathode materials for lithium ion batteries. Electrochim. Acta **52**, 1316–1322 (2006)
19. J. C.Lv, ,Y. Yang, X.Duan Peng, J.Ma, Q. Li, T.Wang ,1D Nb-doped $LiNi_{1/3}Co_{1/3}Mn_{1/3}O_2$ nanostructures as excellent cathodes for Li-ion battery. Electrochim. Acta **297**, 258–266 (2019)
20. M.B.örner D.Becker, R. .Nölle, M.S. Diehl Klein, ,U. Rodehorst, R. Schmuch, M.Winter, T.Placke, Surface modification of Ni-rich $LiNi_{0.8}Co_{0.1}Mn_{0.1}O_2$ cathode material by tungsten oxide coating for improved electrochemical performance in lithium-ion batteries. ACS Appl. Mater. Interfaces **2**, 18404–18414 (2019)
21. J. Liu, B. Reeja-Jayan, A. Manthiram, Conductive surface modification with aluminum of high capacity layered Li [$Li_{0.2}Mn_{0.5}4Ni_{0.13}Co_{0.13}$] O_2 cathodes. J. Phys. Chem. C **114**, 9528–9533 (2010)
22. K.Kalaiselvi K, GP.Kalaignan. Structure and electrochemical performance of Samarium substituted $LiNi_{1/3}$ $Mn_{1/3}$ $Co_{1/3}$ O_2 cathode materials for rechargeable lithium-ion batteries. Journal of Materials Science: Materials in Electronics.29, 20703–20709(2018)
23. K.Kalaiselvi K, GP.Kalaignan Yttrium-substituted $LiNi_{0.3}$ $Mn_{0.3}$ $Co_{0.3}$ O_2 cathode material with enhanced cycling stability for rechargeable lithium-ion batteries. Ionics, 991–997(2019)
24. S.C. Yin, Y.H. Rho, I. Swainson, L.F. Nazar, X-ray/Neutron Diffraction and Electrochemical Studies of LithiumDe/Re-Intercalation in Li1-*x*$Co_{1/3}Ni_{1/3}Mn_{1/3}O_2$ (x = 0 TO 1). Chem. Mater. **18**, 1901–1910 (2006)
25. S.K.Hu,G.H. .Cheng, M.Y. Cheng, B.J. Hwang, ,R. Santhanam, Cycle life improvement of ZrO_2-coated spherical $LiNi_{1/3}Co_{1/3}Mn_{1/3}O_2$ cathode material for lithium ion batteries. Journal of Power Sources. **188**, 564–569 (2009)

26. Z. Han, J.Yu,H.Zhan,X. Liu ,Y. Zhou. Sb_2O_3-modified $LiNi_{1/3}Co_{1/3}Mn_{1/3}O_2$ material with enhanced thermal safety and electrochemical property. Journal of Power Sources. 254, 106–111(2014)
27. D. Bhuvaneswari, N. Kalaiselvi, Comparison of corn starch-assisted sol–gel and combustion methods to prepare LiMn x Co y Ni z O_2 compounds. Journal of Solid State Electrochemistry. **17**, 9–17 (2013)
28. S. Premlatha, M. Chandrasekaran, G.R. Bapu, Preparation of cobalt-RuO_2 nanocomposite modified electrode for highly sensitive and selective determination of hydroxylamine. Sens. Actuators B **252**, 375–384 (2017)
29. S. Premlatha, G.R. Bapu, Direct current electrodeposition of Co-ITO nanoflakes modified steel electrode for highly selective non enzymatic detection of catechol. J. Alloy. Compd. **767**, 622–631 (2018)
30. C. Cheng, H. Yi, F. Chen, Effect of Cr_2O_3 coating on $LiNi_{1/3}Co_{1/3}Mn_{1/3}O_2$ as cathode for lithium-ion batteries. Journal of electronic materials **43**, 3681–3687 (2014)
31. K.C. Mahesh, H. Manjunatha, T.V. Venkatesha, G.S. Suresh, Study of lithium ion intercalation/de-intercalation into $LiNi_{1/3}Co_{1/3}Mn_{1/3}O_2$ in aqueous solution using electrochemical impedance spectroscopy. Journal of solid state electrochemistry **16**, 3011–3025 (2012)
32. J.J. JW.Kim, E. .Travis, K.W. .Hu, S.C. Nam, C.S. Kim. ,J.H. Kang, X.Q. Woo, S.M.George Yang, KH.Oh, SJ.Cho, Unexpected high power performance of atomic layer deposition coated Li $[LiNi_{1/3}Co_{1/3}Mn_{1/3}]$ O_2 cathodes. J. Power Sources **254**, 190–197 (2014)
33. W. Zhu, Z. Zhuang, Z. Lin, Y. Yang, Y. Lin, Z. Huang, Enhanced electrochemical properties and thermal stability of $LiNi_{1/3}Co_{1/3}Mn_{1/3}O_2$ by surface modification with Eu_2 $O_{3,}$ Ionics, 22,1533–1540(2016)
34. P.R. Ilango, T. Subburaj, K. Prasanna, Y.N. Jo, C.W. Lee, Physical and electrochemical performance of PR cathodes coated by Sb_2O_3 using a sol–gel process. Mater. Chem. Phys. **158**, 45–51 (2015)
35. B. Song, M.O. Lai, L. Lu, Influence of Ru substitution on Li-rich 0.55Li2MnO3·0.45$LiNi_{1/3}Co_{1/3}Mn_{1/3}O_2$ cathode for Li-ion batteries. Electrochim. Acta **80**, 187–195 (2012)

Figures

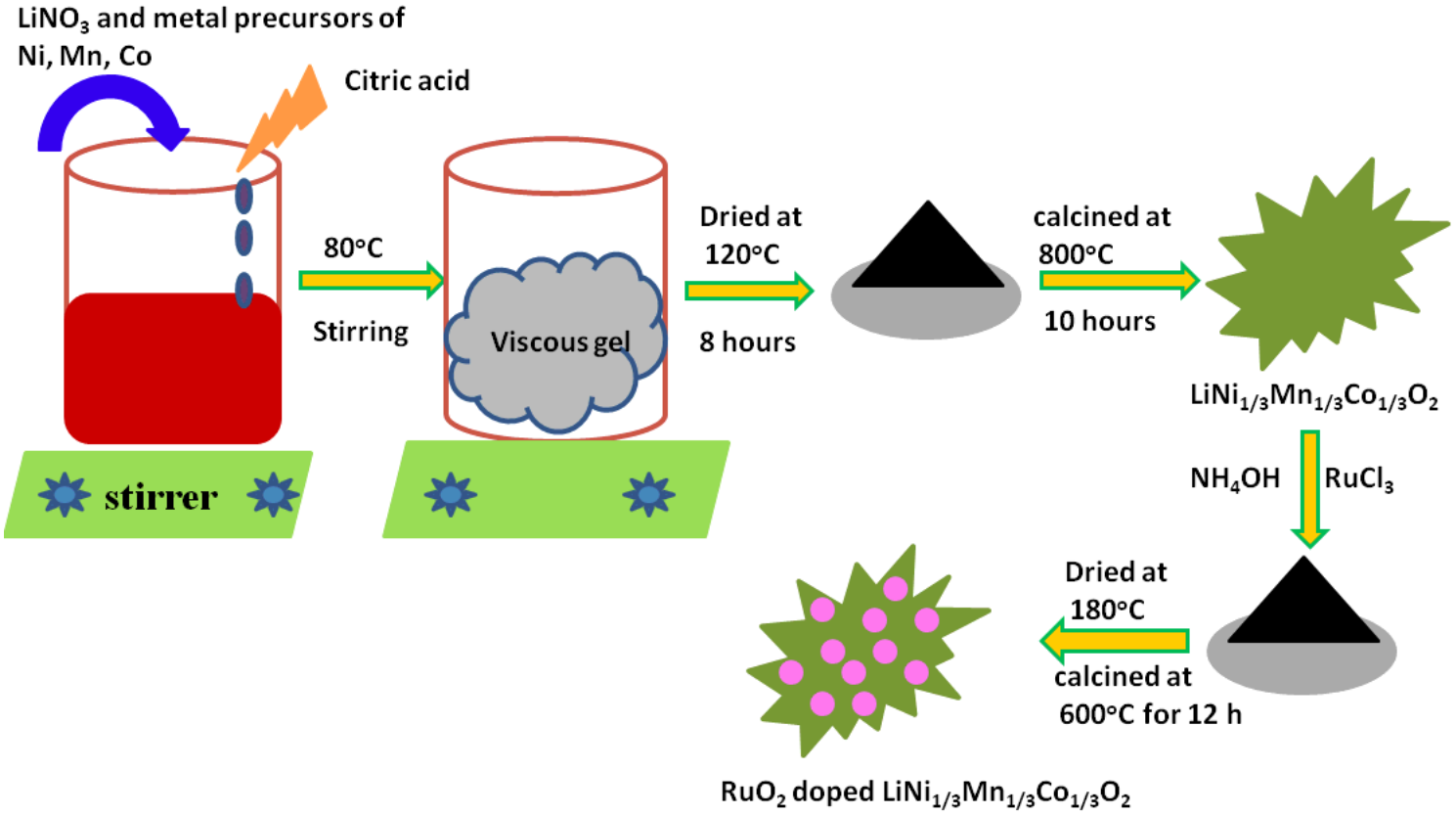

Figure 1

Schematic illustration of the preparation procedure of RuO2 doped LiNi1/3Mn1/3Co1/3O2.

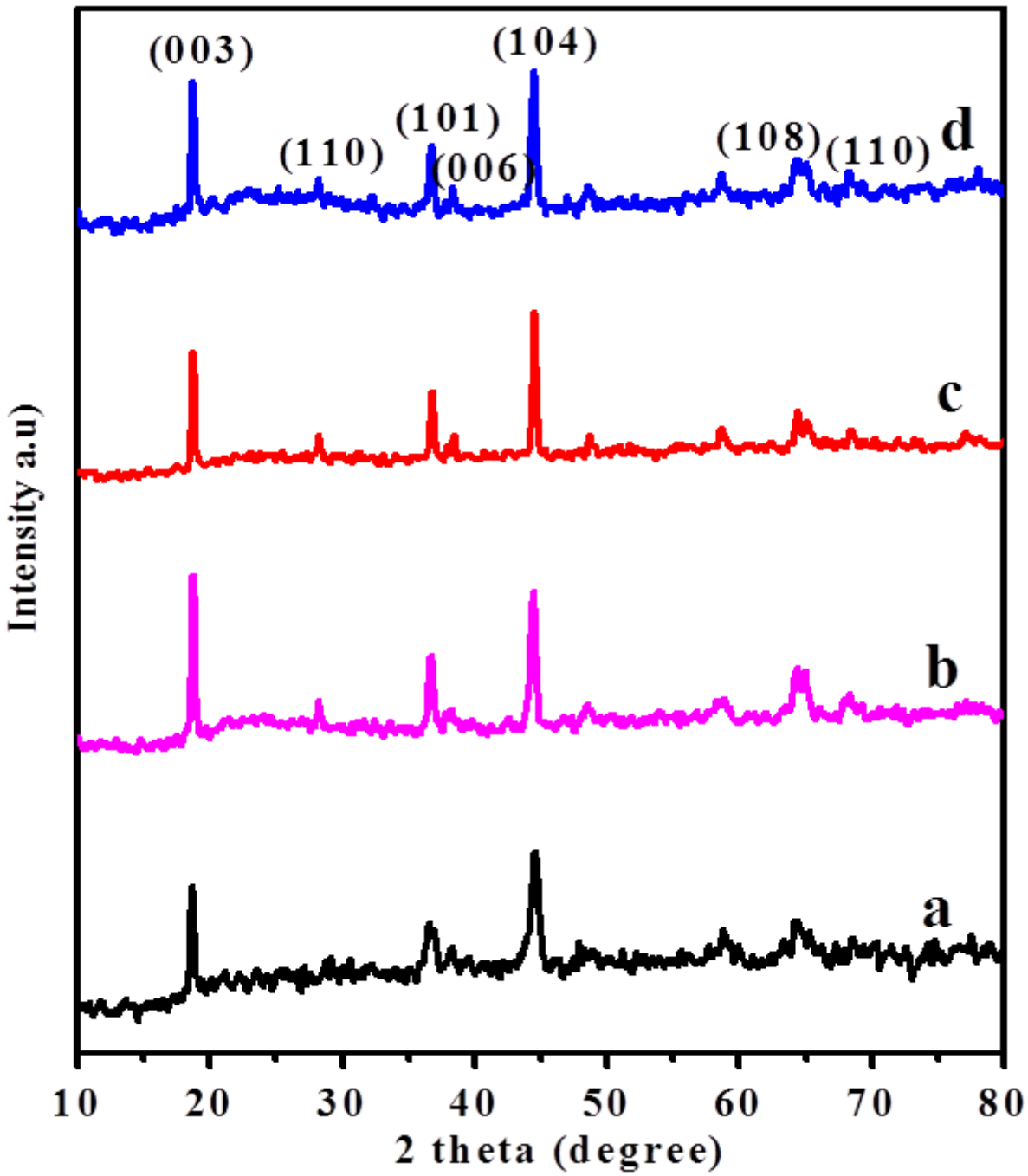

Figure 2

XRD patterns of a) Pristine LiNi1/3Mn1/3Co1/3O2 b) 1% RuO2 doped LiNi1/3Mn1/3Co1/3O2, c) 2% RuO2 doped LiNi1/3Mn1/3Co1/3O2, and d) 3% RuO2 doped LiNi1/3Mn1/3Co1/3O2, cathode materials.

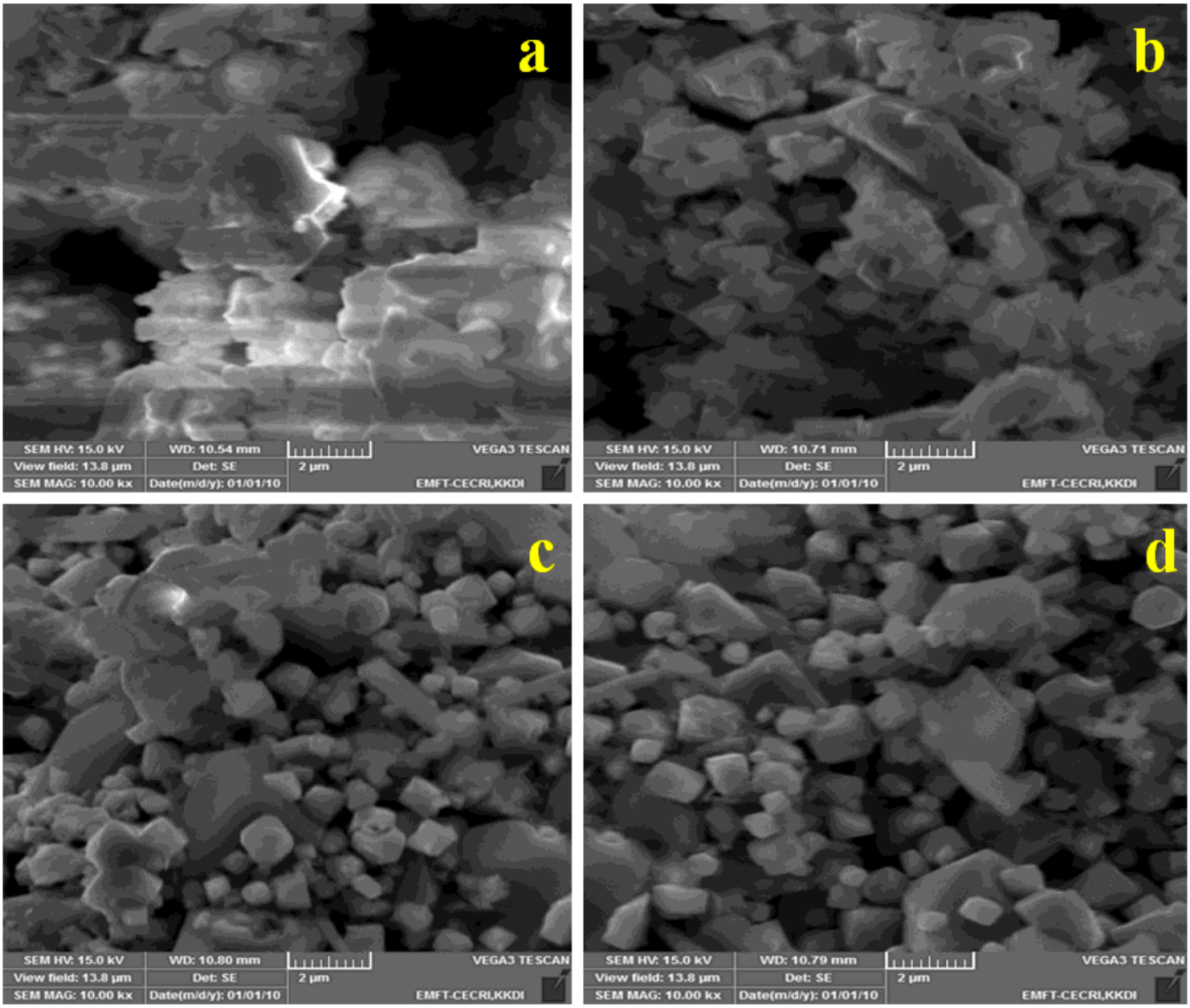

Figure 3

SEM images of a) Pristine LiNi1/3Mn1/3Co1/3O2 b) 1% RuO2 doped LiNi1/3Mn1/3Co1/3O2, c) 2% RuO2 doped LiNi1/3Mn1/3Co1/3O2, and d) 3% RuO2 doped LiNi1/3Mn1/3Co1/3O2.

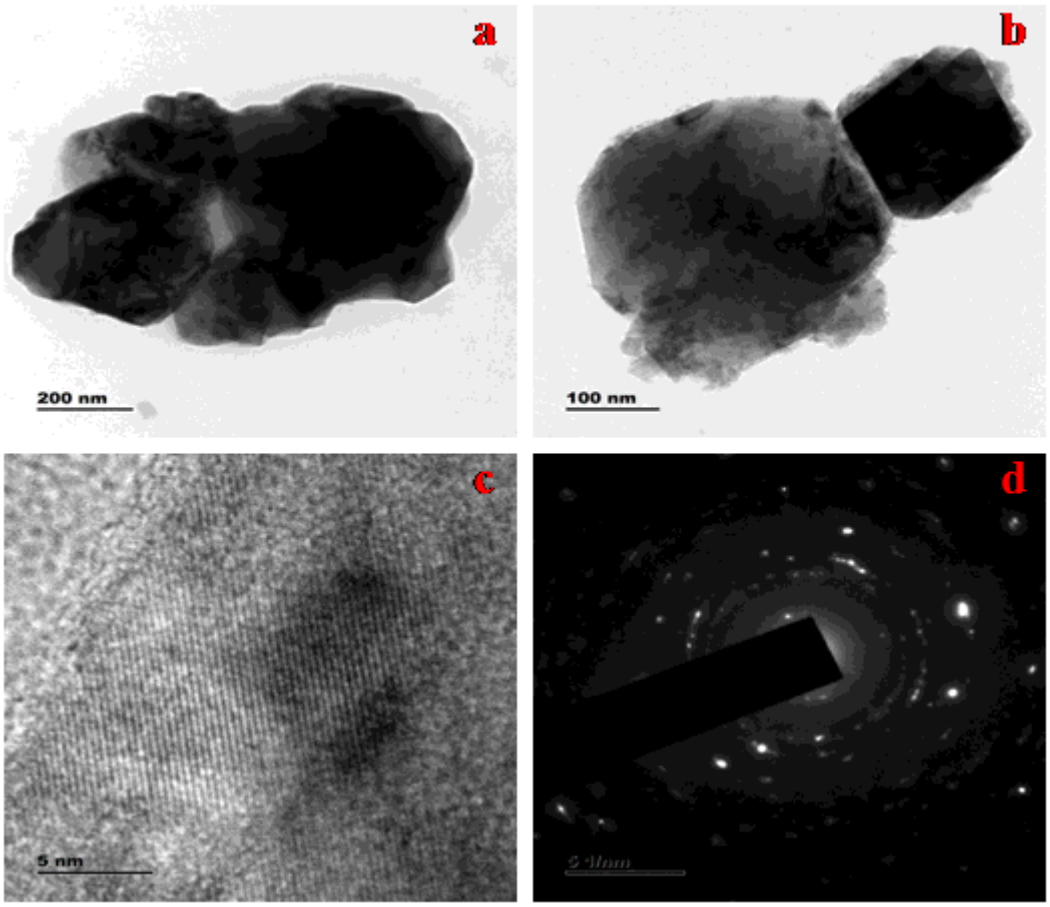

Figure 4

TEM images of a) Pristine LiNi1/3Mn1/3Co1/3O2 b) 3% RuO2 doped LiNi1/3Mn1/3Co1/3O2 c) Lattice fringes d) SAED pattern of 3% RuO2 doped LiNi1/3Mn1/3Co1/3O2.

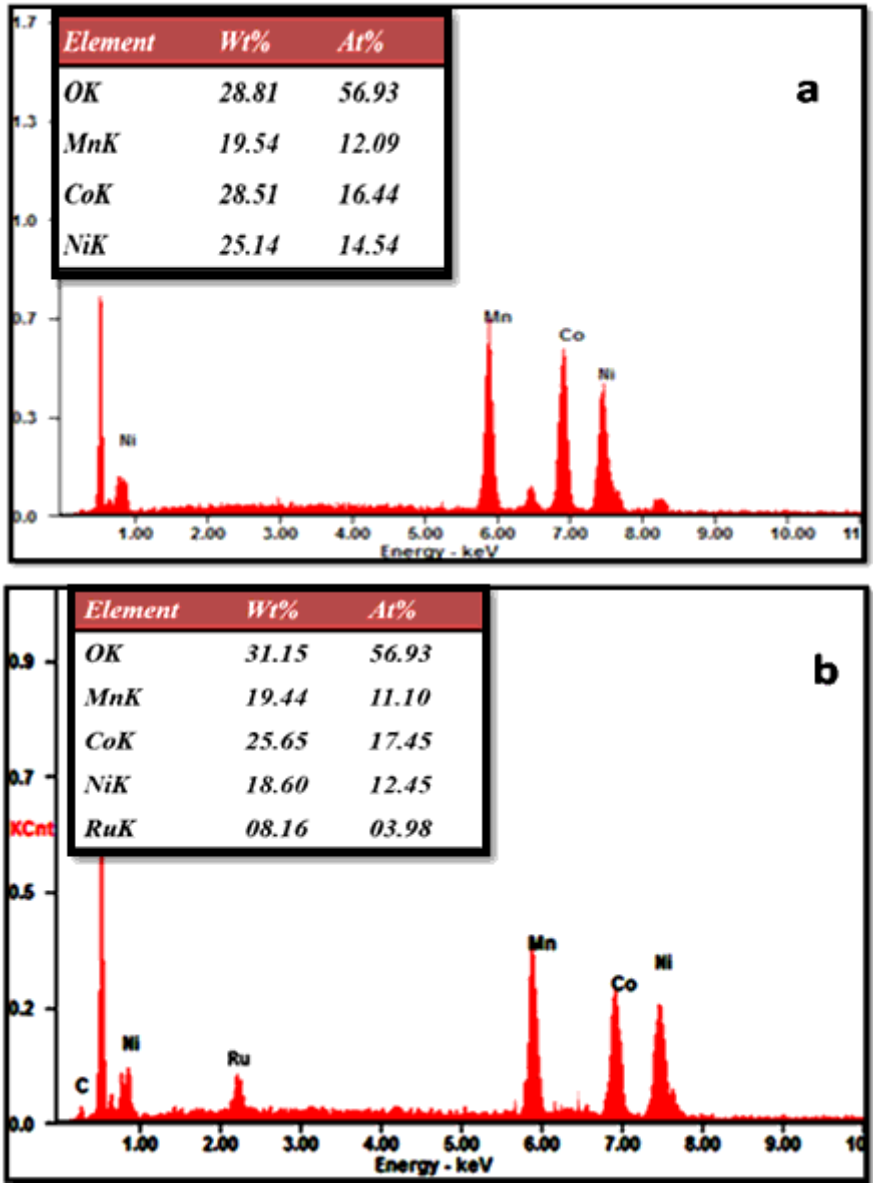

Figure 5

EDX analysis of a) Pristine LiNi1/3Mn1/3Co1/3O2 b) 3% RuO2 doped LiNi1/3Mn1/3Co1/3O2.

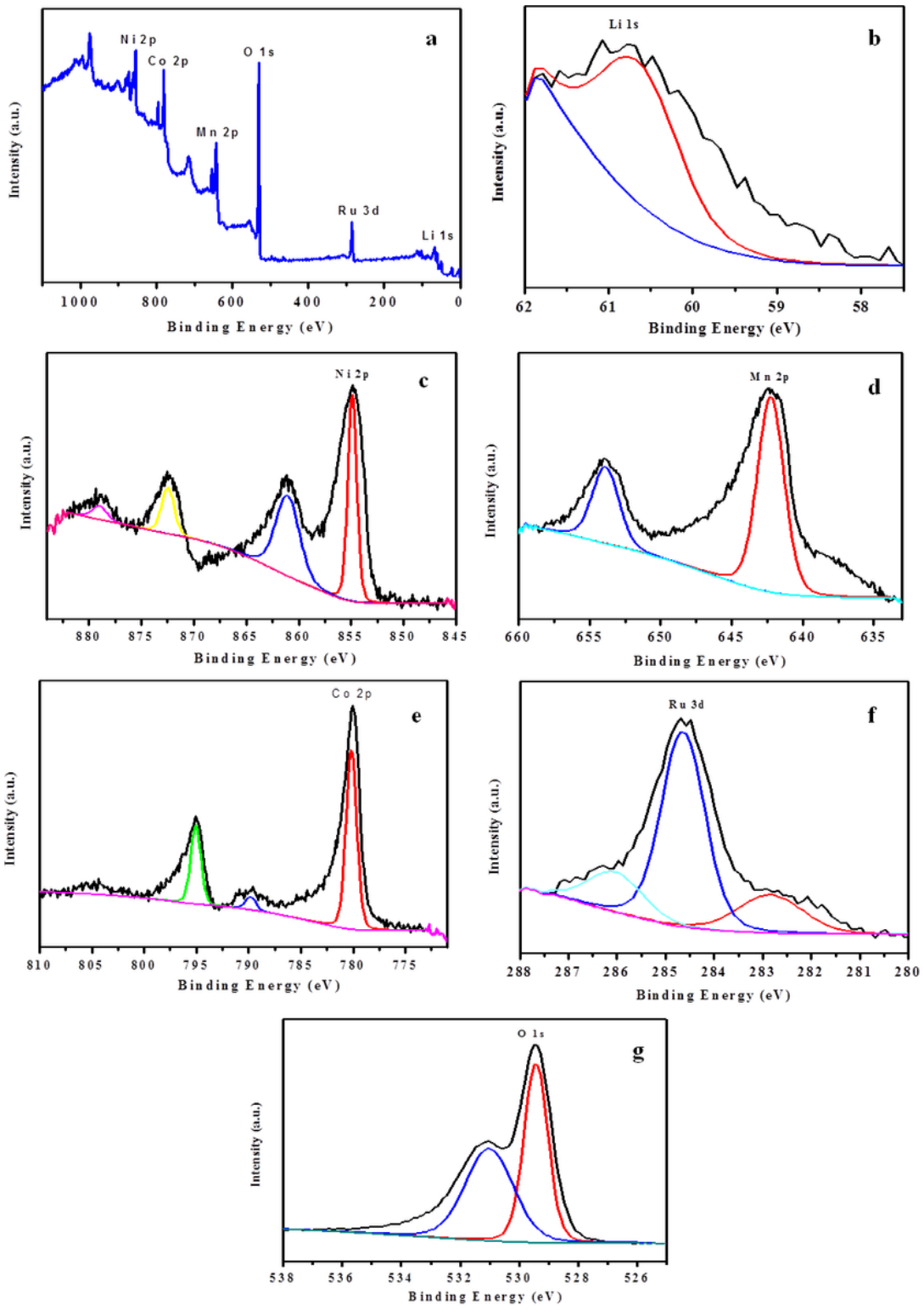

Figure 6

Deconvoluted XPS spectra of 3% RuO2 doped LiNi1/3Mn1/3Co1/3O2 a) survey spectrum b) Li 1s c) Ni 2p d) Mn 2p e) Co 2p f) Ru 3d g) O1s.

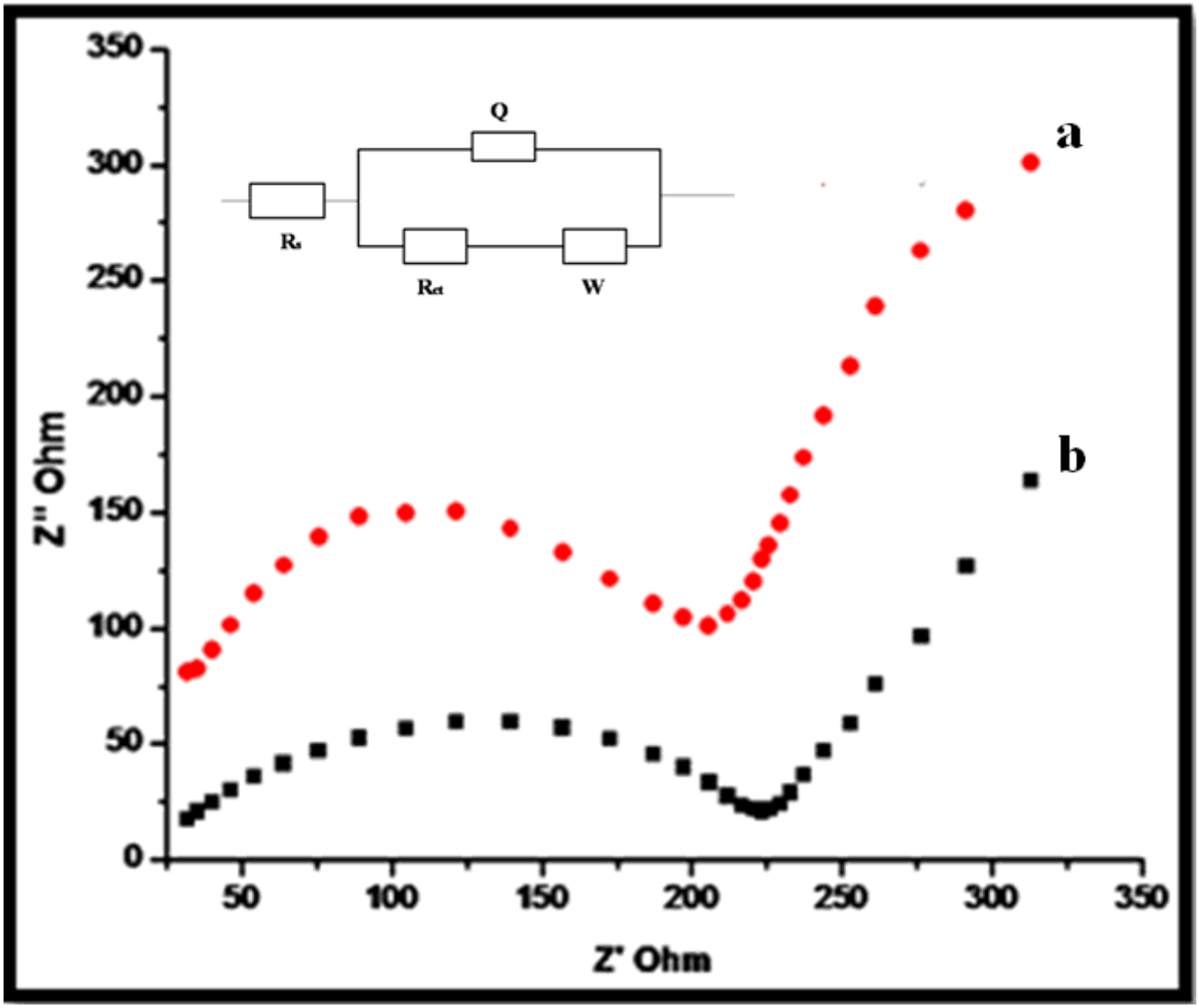

Figure 7

Electrochemical impedance spectra of LiNi1/3Mn1/3Co1/3O2 and 3% RuO2 doped LiNi1/3Mn1/3Co1/3O2. Inset: Equivalent circuit.

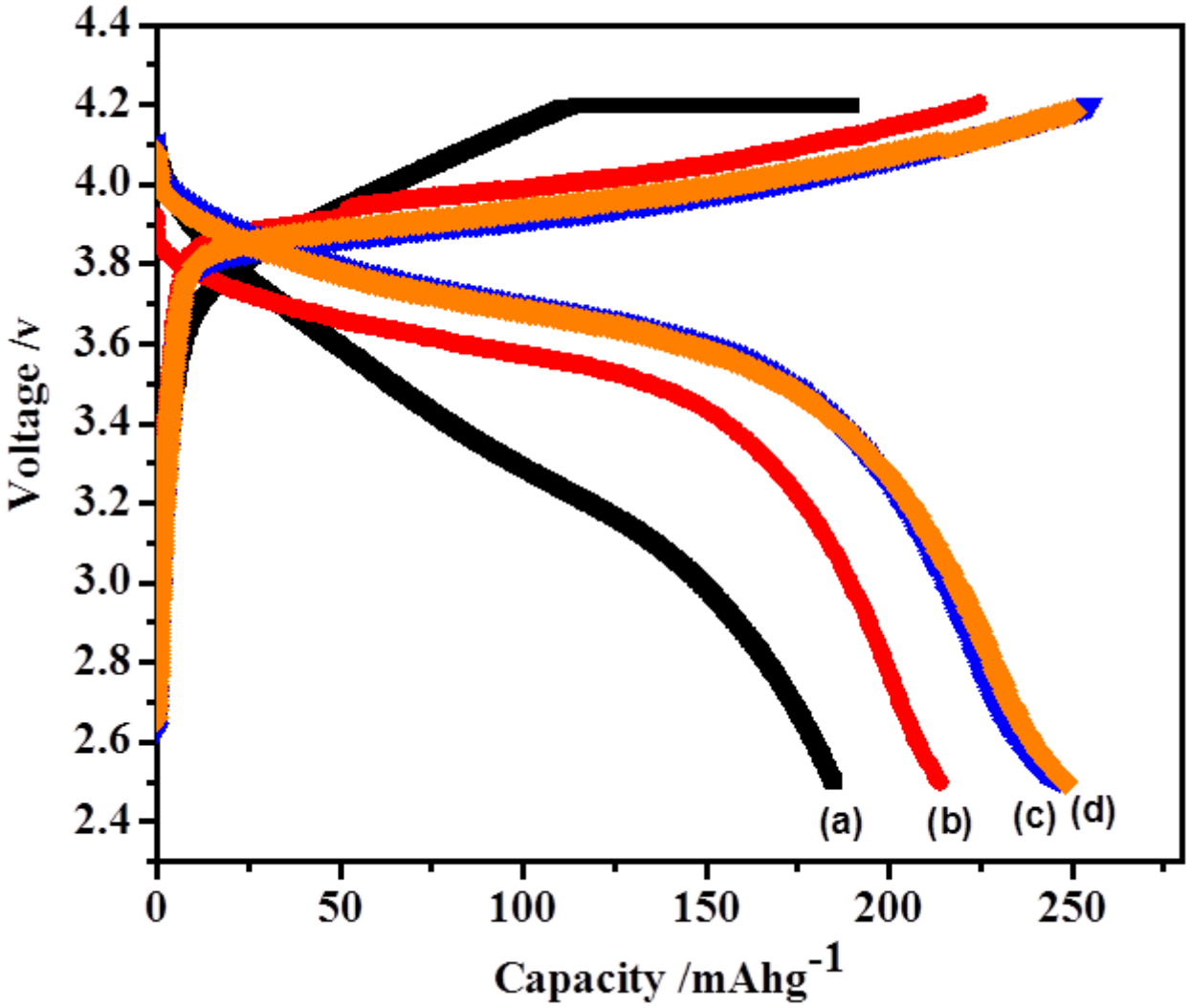

Figure 8

Galvanostatic charge/discharge test of a) pristine LiNi1/3Co1/3Mn1/3O2 b) 1 % RuO2 doped LiNi1/3Co1/3Mn1/3O2 c) 2 % RuO2 doped LiNi1/3Co1/3Mn1/3O2 d) 3% RuO2 doped LiNi1/3Mn1/3Co1/3O2 at 0.1 C rate.

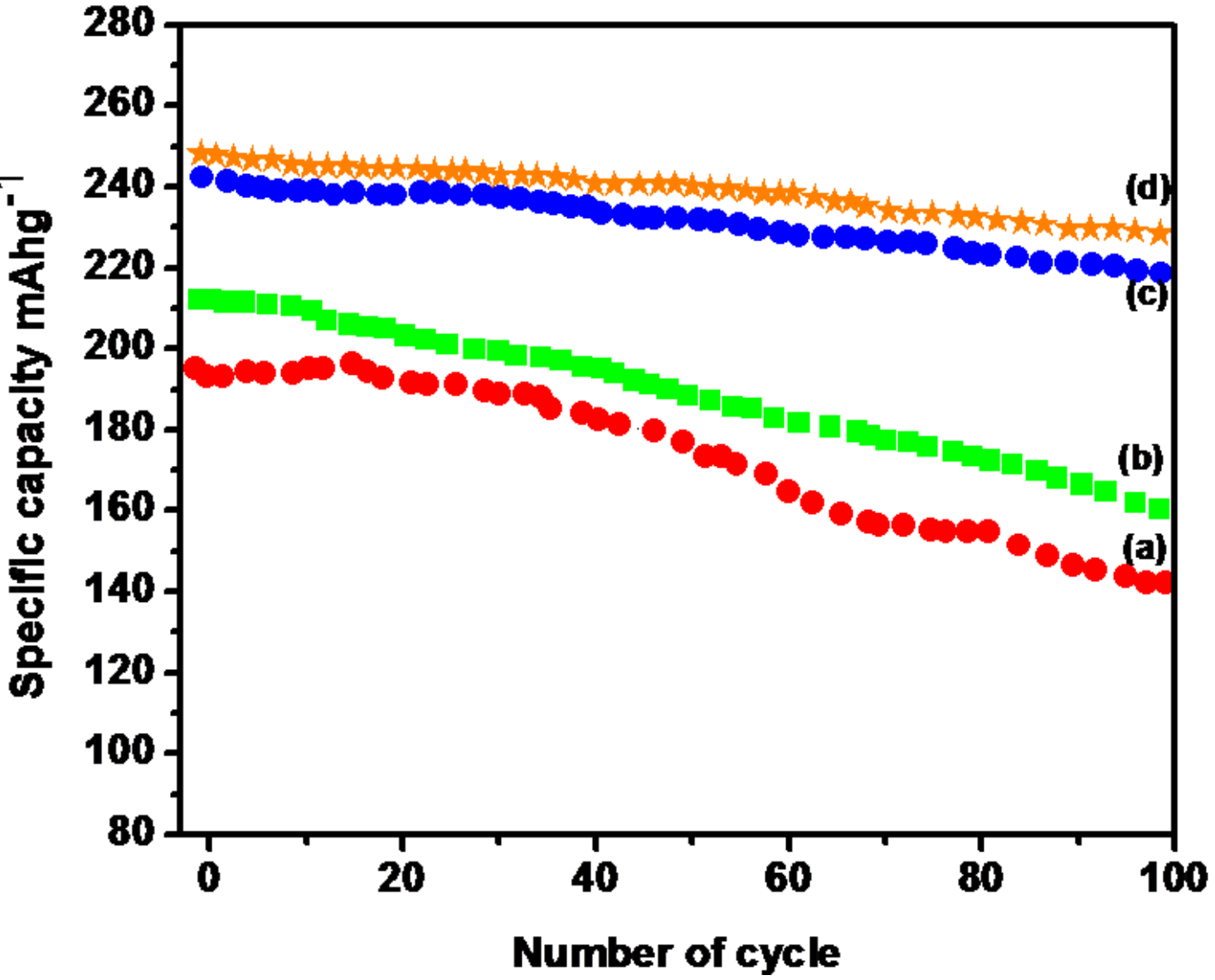

Figure 9

Cyclic performance of a) pristine LiNi1/3Co1/3Mn1/3O2 b) 1% RuO2 LiNi1/3Co1/3Mn1/3O2 c) 2% RuO2 doped LiNi1/3Co1/3Mn1/3O2 d) 3 % RuO2 doped LiNi1/3Co1/3Mn1/3O2 at 0.1 C rate.

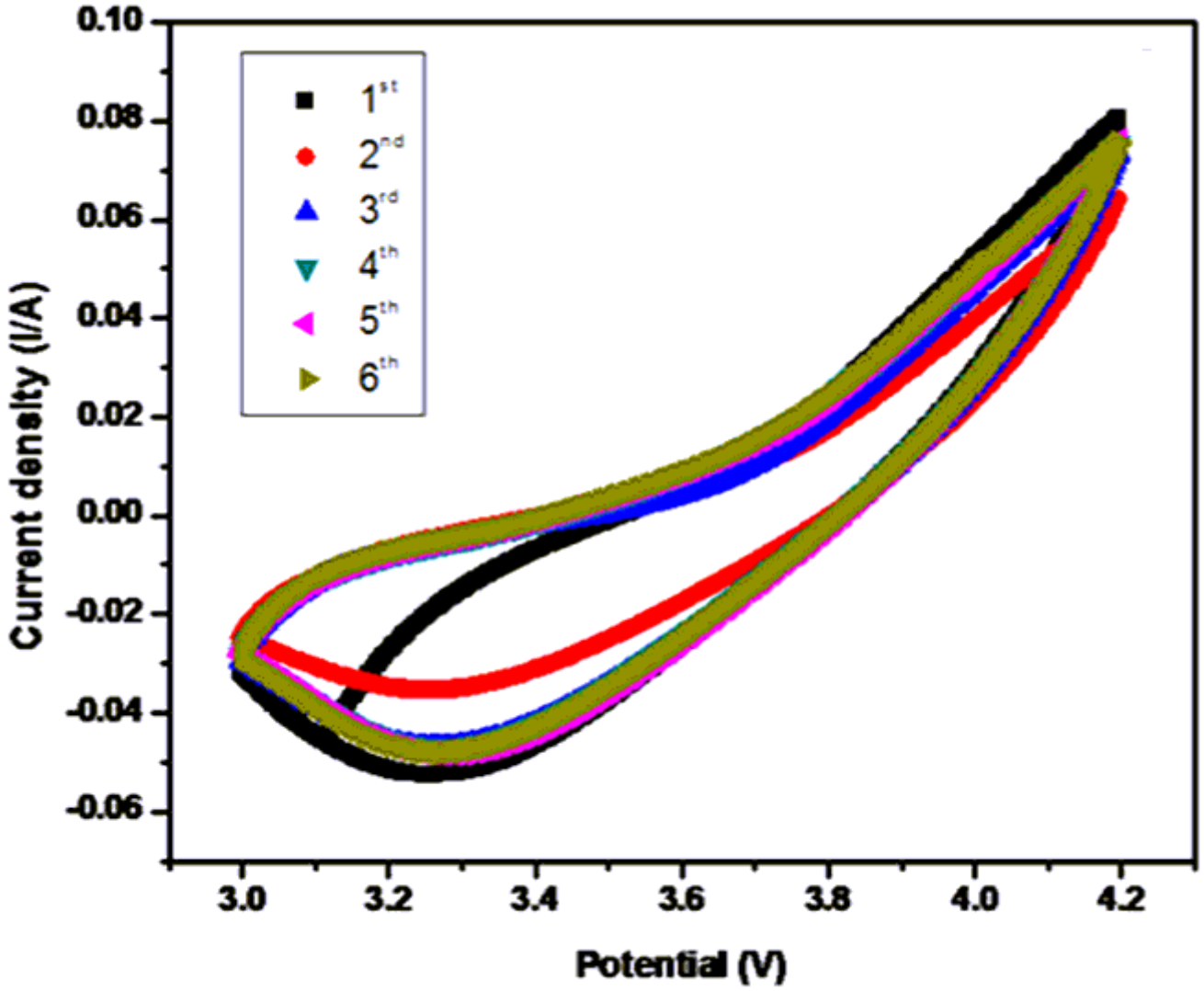

Figure 10

Cyclic voltammograms of 3 % RuO2 doped LiNi1/3Mn1/3Co1/3O2 cathode materials.